NACA

RESEARCH MEMORANDUM

FREE-FLIGHT MEASUREMENTS OF THE ZERO-LIFT DRAG OF SEVERAL

WINGS AT MACH NUMBERS FROM 1.4 TO 3.8

By H. Herbert Jackson

Langley Aeronautical Laboratory
Langley Field, Va.

NATIONAL ADVISORY COMMITTEE
FOR AERONAUTICS
WASHINGTON
June 22, 1956

NATIONAL ADVISORY COMMITTEE FOR AERONAUTICS

RESEARCH MEMORANDUM

FREE-FLIGHT MEASUREMENTS OF THE ZERO-LIFT DRAG OF SEVERAL

WINGS AT MACH NUMBERS FROM 1.4 TO 3.8

By H. Herbert Jackson

SUMMARY·

The zero-lift drag of several wings of current interest has been
obtained at supersonic Mach numbers from 1.4 to 3.8 in free flight with
rocket-propelled models. The wings tested were all of the same exposed
area, mounted on the same basic body configuration, and consisted of a
swept, tapered wing of 5-percent hexagonal section, a swept, tapered wing
with NACA 65A004 airfoil section, an unswept wing with NACA 65A004.5 air-
foil section, a 60° delta wing with NACA 65A003 airfoil section, and
a 40.78° diamond wing with NACA 65A003 airfoil section.

Of the wings tested, the 3-percent-thick delta and diamond wings
had the lowest drag, the drag coefficients of the two wings being the
same and showing very little change with Mach numbers from 2.4 to 3.8.
Changing the section of otherwise identical swept, tapered wings from
a 5-percent-thick hexagonal section to an NACA 65A004 section resulted
in a 50- to 25-percent reduction in drag at Mach numbers of 2.4 and 3.4,
respectively. Newtonian impact theory gave good approximations of the
pressure drag for all the wings tested at the high Mach numbers and for
the wings with blunt leading edge over the entire Mach number range.
The percentages of wing-plus-interference drag accounted for by the pres-
sure drag are approximately 70 percent for the 5-percent-thick swept,
tapered slab wing, 60 percent for the swept, tapered wing with NACA 65A004
airfoil section, 75 percent for the unswept, tapered wing with NACA
65A004.5 airfoil section, and 53 percent for the delta wing and diamond
wing with NACA 65A003 sections.

INTRODUCTION

The increase in speed of aircraft has shown the need for large-
scale experimental data on the drag of wings at high supersonic speeds.
In order to provide some information in this range, the Pilotless Aircraft

Research Division of the Langley Aeronautical Laboratory has conducted a free-flight investigation of the drag of several wings of current interest at Mach numbers extending to 4.0.

This paper presents the zero-lift drag and base pressure results on five wing-body models and two wingless models in free flight at large Reynolds numbers. In order to do away with any effect of body size and shape on the wing drag information, the same basic body was used on all test models. The exposed wing areas of the various wing configurations investigated also remained the same in order to make the drag results more comparable.

The tests covered a Mach number range from 1.4 to 4.0, which corresponds to a Reynolds number range of 0.5×10^6 to 18×10^6 based on a length of 1 foot or a Reynolds number range of 2×10^6 to 35×10^6 based on the mean aerodynamic chords of the exposed wings.

SYMBOLS

C_D drag coefficient based on S_{w_e}

C_{D_T} total configuration drag coefficient

C_{D_W} wing-plus-interference drag coefficient

C_{D_p} wing pressure drag coefficient

C_{D_b} base drag coefficient, $-C_{p_b}\left(\dfrac{S_b}{S_{w_e}}\right)$

$C_{D_{Fin}}$ fin drag coefficient of two fins based on S_{w_e}

C_{p_b} body base pressure coefficient, $\dfrac{p_b - p_o}{q}$

p_b body base pressure, lb/sq ft

p_o atmospheric static pressure, lb/sq ft

q dynamic pressure, lb/sq ft

M   Mach number

R   test Reynolds number, based on a length of 1 foot

Λ wing sweepback angle, deg

A   wing aspect ratio, b^2/S_{w_e}

λ wing taper ratio, c_t/c_r

b   exposed wing span

c_t wing tip chord

c_r wing root chord at body junction

S_w wing plan-form area to center line of model, sq ft

S_{w_e} exposed wing plan-form area, 5.556 sq ft

S_f body frontal area, sq ft

S_b base area, sq ft

S_{Fin} exposed area of one fin, sq ft

t   wing thickness

c   local wing chord, streamwise

r   local body radius at any station, in.

x   distance from station 0, in.

Subscripts:

LE   leading edge

TE   trailing edge

MODELS AND TESTS

The general arrangement and basic geometry of the configurations investigated are given in figure 1 and table I. A photograph of a wingless model with 4 fins and one with swept, tapered wings mounted on the model is shown in figure 2.

The basic test vehicles were cylinders with parabolic noses of fineness ratio 6.03 and short conical afterbodies. The bodies had a total fineness ratio of 18.75, frontal area of 0.184 square foot, and base area of 0.136 square foot. A pitot tube measuring both total pressure and static pressure extended from the nose of each model.

All test models were stabilized by 5-percent-thick, hexagonal, swept, tapered tail fins, four on the models without wings (models 1a and 1b) and two on the models with wings. The wings tested were all of the same exposed area and consisted of a swept, tapered wing of 5-percent-thick hexagonal section (model 2), a swept, tapered wing with NACA 65A004 section (model 3), an unswept wing with NACA 65A004.5 section (model 4), a 60° delta wing with NACA 65A003 section (model 5), and a 40.70° diamond wing with NACA 65A003 section (model 6). All the wings were located as far rearward as possible to keep the trim changes small and to include them within the Mach cone of the body nose so that the body nose interference was similar for all wings.

The bodies and test wings of the models were constructed of magnesium alloy, with all the wings except the swept, tapered, 5-percent-thick, hexagonal wing being solid. Considerations of the severity of the temperature effects resulting from the flight conditions indicated that there would be no serious effect on the bodies and wings.

A two-stage propulsion system was employed for all models, with a variety of first-stage booster rocket motors (table I) used to propel the various models to supersonic speeds. For the second stage, all models utilized a 5-inch-diameter HPAG rocket motor installed in the fuselage for propulsion to higher supersonic speeds. Photographs of two models and boosters on the launchers are shown in figure 3. All the models were launched at approximately 70° from the horizontal.

Contained within each model was a telemeter which measured longitudinal acceleration, total pressure, static pressure, and base pressure. The base pressure was measured from orifices located as shown in figure 4.

Ground instrumentation was also used to record the model flight and consisted of CW Doppler velocimeter radar for measuring model speed, NACA modified SCR 584 radar tracking unit for measuring trajectory, and radiosonde units for measuring air pressure and temperature from which

speed of sound, density, viscosity, and altitudes were obtained. The model speeds determined by the CW Doppler velocimeter were supplemented with speeds determined by integrating the model decelerations with time obtained from telemetry of longitudinal accelerations and by velocities obtained by the use of total and static pressures. Velocity and total drag were obtained from CW Doppler radar and corrected for winds aloft as described in reference 1. All the test data presented herein were obtained during the deceleration portions of flight.

The error in drag coefficient C_D is estimated to be within ±0.0007 and the error in Mach number is estimated to be within ±0.005.

The errors in wing-plus-interference drag coefficients obtained by subtracting fuselage drag and base drag from wing-fuselage drag may be somewhat larger. A typical set of test results is shown in figure 5 to illustrate the continuity and scatter of data.

RESULTS AND DISCUSSION

General Discussion

The variation of Reynolds number, based on a length of 1 foot, with Mach number for the test models is shown in figure 6. The differences in Reynolds number shown from one model to another were caused primarily by the different altitudes attained. The overlap of the drag-coefficient data for models 1a and 1b, shown in figure 5, indicates negligible effect of the differences in Reynolds numbers on the drag coefficients. All drag coefficients are based on an exposed wing area of 5.556 square feet, the exposed areas of all wings being the same.

The results for each model are presented in figure 7, wherein are plotted the total-drag coefficient C_{D_T} and base-drag coefficients C_{D_b}. For some models, the faired curves of the coefficients were extrapolated beyond actual data (as shown in fig. 7) in order to obtain extended wing-plus-interference drags. The extrapolations were accomplished by maintaining the curvature of the experimental data.

Shown in figure 8 are the experimentally determined fin drag coefficients and the drag coefficient for the body plus two fins. The curves labeled "wing-plus-interference (fin as wings)" and "2 fins" were obtained from flight tests of two four-fin wingless bodies (models 1a and 1b) and of a winged body with two fins (model 2) having wings which were scaled-up versions of the fins and had the same exposed wing area as all the other wings tested. The fin drag coefficient was obtained from the following expression:

$$C_{D_{Fin}} = \frac{\left(C_{D_T} - C_{D_b}\right)_{winged} - \left(C_{D_T} - C_{D_b}\right)_{wingless}}{\left(\dfrac{S_{W_e}}{2S_{Fin}} - 1\right)}$$

which is valid for the case where the wings were scaled-up versions of the fins and where the effects of Reynolds number due to the different wing chords has been neglected. Actually, the Reynolds number differences would cause very little error in the resulting wing-plus-interference drag coefficients. For the general case, the wing-plus-interference drag is given by

$$C_{D_W} = \left(C_{D_T} - C_{D_b}\right)_{winged} - \left(C_{D_T} - C_{D_b}\right)_{wingless} + C_{D_{Fin}}$$

Comparison of Swept, Unswept, Delta, and Diamond Wings

The total-drag coefficients and corresponding wing-plus-interference drag coefficients of the models with swept, tapered wings (models 2 and 3), unswept, tapered wings (model 4), delta wings (model 5), and diamond wings (model 6) are compared in figure 9 at the respective flight test Reynolds numbers. As shown in the figure, the 3-percent-thick delta wing and diamond wing, which had the lowest aspect ratio (A = 2.31) and thinnest section, had the lowest drag of the wings tested over the test Mach number range. The slight difference in drag between the delta and diamond wings at the high Mach numbers may be due to the different plan forms. All the wings show a similar trend of decreasing drag coefficient with increasing Mach number over the Mach number range of the tests.

Presented in figures 10 to 12 are the wing pressure-plus-interference drag coefficients for the test wings, obtained by subtracting estimated skin-friction drag coefficients from the experimentally determined wing-plus-interference drag coefficients. The skin-friction drag was estimated with the aid of references 2 and 3, using Reynolds number values based on the exposed mean aerodynamic chords and assuming completely turbulent flow.

Shown in figure 10 is the effect on pressure drag of changing the airfoil section of a swept wing from a 5-percent-thick hexagonal section with a sharp leading edge (model 2) to an NACA 65A004 airfoil section (model 3). As indicated in the figure, the drag at a Mach number of 2.4 of the swept wing with a 5-percent-thick hexagonal section is a little more than twice that of a wing with the same exposed plan form but an NACA 65A004 section; at Mach number 3.4, however, the drag of the wing with 5-percent-thick hexagonal section has reduced to 1.5 times that of a wing with NACA 65A004 section. The percentage of wing-plus-interference

drag accounted for by the pressure drags shown in figure 10 are 80, 66, and 75 percent for the 5-percent-thick, hexagonal-section wing and 55.3, 61.2, and 66.7 percent for the wing with NACA 65A004 airfoil section at Mach numbers of 2.4, 3.0, and 3.4, respectively.

Shown also in figure 10 are the pressure drag coefficients of the 5-percent-thick, hexagonal-section wing and the wing with the NACA 65A004 section as obtained by Newtonian impact theory, reference 4. On comparison with the curves presented in figure 10, it is observed that the impact theory is in somewhat better agreement with experimentally based estimates of the pressure drag at Mach numbers of 2.0 to 4.0 for the blunt-leading-edge wing than for the sharp-leading-edge wing which goes only to $M = 3.4$. This result is probably due to the fact that the flow in the region of the leading edge of the NACA 65A004 airfoil, by virtue of its relative bluntness, has more nearly the characteristics of a truly hypersonic flow than does the flow in the region of the sharp-leading-edge wedge airfoil. It is not expected, of course, that the impact theory should apply accurately at these relatively low Mach numbers and the agreement for the sharp-leading-edge airfoil would undoubtedly be better at somewhat higher Mach numbers than those presented.

Presented in figure 11 is a comparison of the pressure-plus-interference drag coefficients of the unswept, tapered wing with NACA 65A004.5 airfoil section (model 4) with those for model 12 of reference 5 (a wing of the same plan form and section). In order to make comparison possible, it was necessary that the drag coefficients of reference 5, which are based on total wing area, be converted to exposed wing area. The agreement is not quite as good as would be expected, but part of the disagreement may result from the fact that the reference body has considerably higher interference drag than the present test vehicle. The pressure drag shown in figure 11 for model 4 accounts for approximately 75 percent of the wing-plus-interference drag.

Also shown in figure 11 is the pressure drag coefficient for the NACA 65A004.5 airfoil wing as obtained by Newtonian theory. It is indicated that if the experimental curve was extrapolated to Mach number 4.0, the theoretical data would be in good agreement with the experimental data, even at this relatively low Mach number.

Compared in figure 12 are the wing pressure-plus-interference drag coefficients of a delta wing with $\Lambda_{LE} = 60^{\circ}$ and of a diamond wing with $\Lambda_{LE} = 40.87^{\circ}$. Both wings had an NACA 65A003 airfoil section and an exposed aspect ratio of 2.31. As indicated by the figure the drags agreed within the accuracy of the data over the test Mach number range of 2.2 to 3.8. Also presented in figure 12, for comparison and to extend the delta wing drag curve from $M = 1.0$ to 3.8, are the drag data from reference 6 (model 11) and reference 7 (model 5) after subtracting the

skin-friction drag and basing the data on exposed wing area. The agree-
ment between the present test data and the reference data is excellent
in view of the fact that the interference effects might be considerably
different. It is difficult, however, to make any comparison of the
diamond wing from the present test with that of reference 8 (after sub-
tracting the skin friction and basing on exposed wing area) because of
the wide differences in Mach number. The percentage of wing-plus-
interference drag accounted for by the experimentally determined pressure
drags shown in figure 12 are 45.7, 53, and 61.3 percent for the delta
wing at Mach numbers of 2.4, 3.0, and 3.4, respectively, and 53.4 and
58.4 percent for the diamond wing at Mach numbers of 3.0 and 3.4,
respectively.

Presented in figure 13, for comparison with the experimentally
determined wing pressure drags of the delta wing and diamond wing
(presented in fig. 12), is the variation of pressure drag with Mach
number as obtained by linearized theory (ref. 9) for a supersonic leading
edge and by Newtonian impact theory. Inasmuch as the linearized theory
does not strictly apply for the rounded leading edges, it was necessary
to assume sharp leading edges for the wings. This assumption was made
by using the average slope over the first 5 percent of the wing chords.
Comparison of the theory with figure 12 indicates that whereas linear
theory gives low approximations of the pressure drags above M = 2.0,
the Newtonian theory closely approximates the experimentally determined
drags, even at these relatively low Mach numbers.

Since most of the test data were obtained at Mach numbers for which
the leading edges of the wings are supersonic, no attempt was made to
apply theoretical area rule predictions to the wing pressure drags. Such
theoretical pressure drags would not be any more accurate than those
which were obtained from the linearized wing theory, because it is
necessary to assume sharp leading edges in both cases. Also, in the
tests presented herein, the interference effects between the wings and
bodies would be expected to be small because of the relatively small
body and high Mach numbers of the tests.

In figure 14 are presented base pressure coefficients against Mach
number for the wingless and winged models tested. There appears to be
very little effect of the presence and shape of the wings on base pres-
sure at Mach numbers above 2.4. The irregularities indicated at the
lower Mach numbers are no doubt due to instrument inaccuracies at the
higher altitudes.

(

CONCLUSIONS

The present investigation made to determine the zero-lift drag at high supersonic Mach numbers of several wings of current interest indicated the following:

1. The 60° delta and 40.87° diamond wings with NACA 65A003 sections and aspect ratio of 2.31 had the lowest drag of the wings tested over the test Mach number range.

2. Changing the airfoil section of otherwise identical swept, tapered wings from a 5-percent-thick hexagonal section to an NACA 65A004 section resulted in a 50-percent reduction in wing wave drag at a Mach number of 2.4 and a 25-percent reduction at a Mach number of 3.4.

3. Newtonian impact theory gave good approximations of the pressure drag for all the wings tested at the high Mach numbers and for the blunt-leading-edge wings over the entire Mach number range.

4. The percentage of wing-plus-interference drag accounted for by the pressure drag is approximately 70 percent for the 5-percent-thick swept, tapered slab wing, 60 percent for the swept, tapered wing with NACA 65A004 section, 75 percent for the unswept, tapered wing with NACA 65A004.5 section, and 53 percent for the delta wing and diamond wing with NACA 65A003 sections.

Langley Aeronautical Laboratory,
    National Advisory Committee for Aeronautics,
        Langley Field, Va., February 17, 1956.

REFERENCES

1. Wallskog, Harvey A., and Hart, Roger G.: Investigation of the Drag of Blunt-Nosed Bodies of Revolution in Free Flight at Mach Numbers From 0.6 to 2.3. NACA RM L53D14a, 1953.

2. Van Driest, E. R.: Turbulent Boundary Layer in Compressible Fluids. Jour. Aero. Sci., vol. 18, no. 3, Mar. 1951, pp. 145-160, 216.

3. Rubesin, Morris W., Maydew, Randall C., and Varga, Steven A.: An Analytical and Experimental Investigation of the Skin Friction of the Turbulent Boundary Layer on a Flat Plate at Supersonic Speeds. NACA TN 2305, 1951.

4. Grimminger, G., Williams, E. P., and Young, G. B. W.: Lift on Inclined Bodies of Revolution in Hypersonic Flow. Jour. Aero. Sci., vol. 17, no. 11, Nov. 1950, pp. 675-690.

5. Morrow, John D., and Nelson, Robert L.: Large-Scale Flight Measurements of Zero-Lift Drag of 10 Wing-Body Configurations at Mach Numbers From 0.8 to 1.6. NACA RM L52D18a, 1953.

6. Sandahl, Carl A., and Stoney, William E., Jr.: Effect of Some Section Modifications and Protuberances on the Zero-Lift Drag of Delta Wings at Transonic and Supersonic Speeds. NACA RM L53L24a, 1953.

7. Hopko, Russell N., and Sandahl, Carl A.: Free-Flight Investigation of the Zero-Lift Drag of Several Wings at Supersonic Mach Numbers Extending to 2.6. NACA RM L52D29, 1952.

8. Wallskog, Harvey A., and Morrow, John D.: Large-Scale Flight Measurements of Zero-Lift Drag and Low-Lift Longitudinal Characteristics of a Diamond-Wing—Body Combination at Mach Numbers from 0.725 to 1.54. NACA RM L53C17, 1953.

9. Grant, Frederich C., and Cooper, Morton: Tables For the Computation of Wave Drag of Arrow Wing at Arbitrary Airfoil Section. NACA TN 3185, 1954.

TABLE I

GEOMETRY OF MODELS INVESTIGATED

Model	Designation	Booster	Λ_{LE}, deg	Λ_{TE}, deg	A^*	λ	Airfoil	S_f/β_{w_e}	Mean aerodynamic chord, ft*
1a	Wingless	Double Deacon	-----	-----	---	---	--------------------------	-----	-----
1b	Wingless	Single Deacon	-----	-----	---	---	--------------------------	-----	-----
2	Swept	Quadruple Deacon	56.77	32.38	3.00	0.2	Hexagonal $t/c = 0.05$	0.033	1.562
3	Swept	Nike	56.77	32.38	3.00	.2	NACA 65A004	.033	1.562
4	Unswept	Quadruple Deacon	23.23	-8.17	3.00	.4	NACA 65A004.5	.033	1.444
5	Delta	Quadruple Deacon	60.00	0	2.31	0	NACA 65A003	.033	2.068
6	Diamond	Nike	40.78	-40.78	2.31	0	NACA 65A003	.033	2.070

*All wing parameters are based on exposed wing geometry.

NACA RM L56C13

Nose profile equation:

$$r = 2.90 - \frac{2.90}{35.0^2}(35-x)^2$$

Section A-A
Typical fin section, not to scale
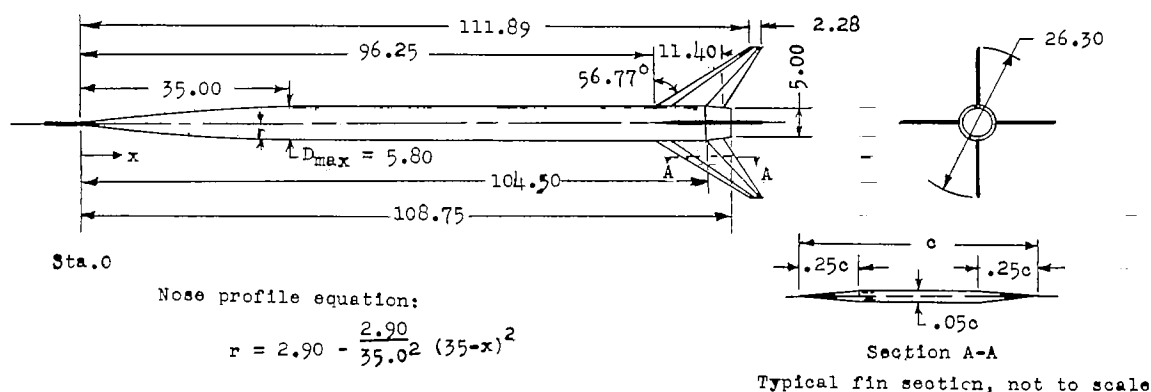
(a) Basic body with 4 fins (models 1a and 1b).

A = 3.00
λ = 0.20
$8_f/S_{W_e} = 0.033$
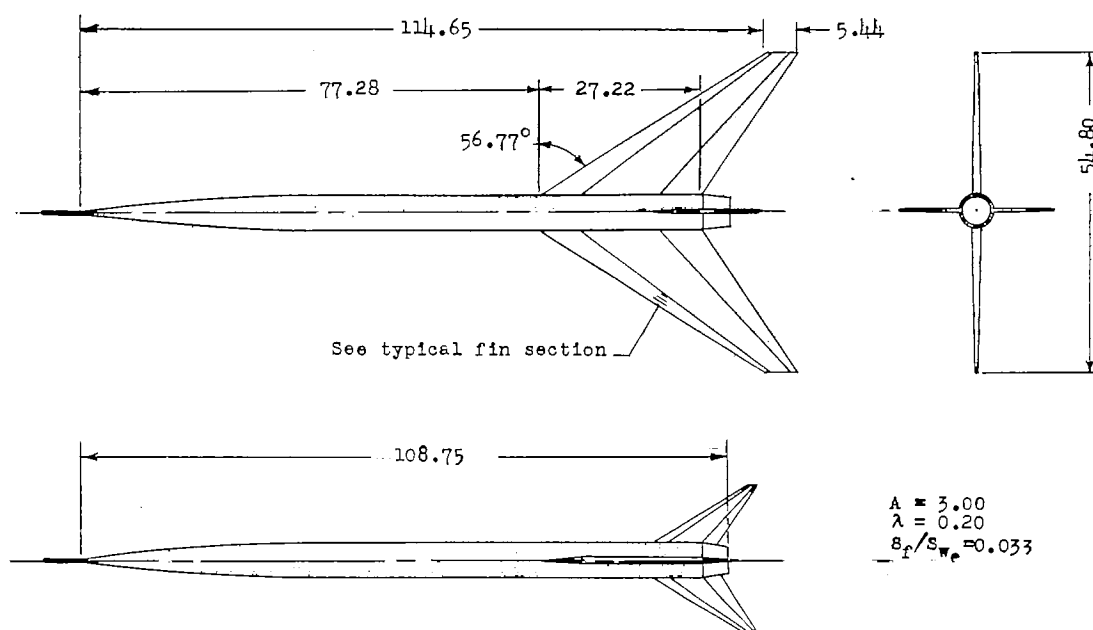
(b) Swept tapered slab wing (fins as wings) on basic body with two fins
(model 2). (Model 3 had same wing dimensions but NACA 65A004 airfoil
sections parallel to free stream.)

Figure 1.- General arrangement of test models. Basic body with two fins
used on all winged models. All dimensions are in inches.
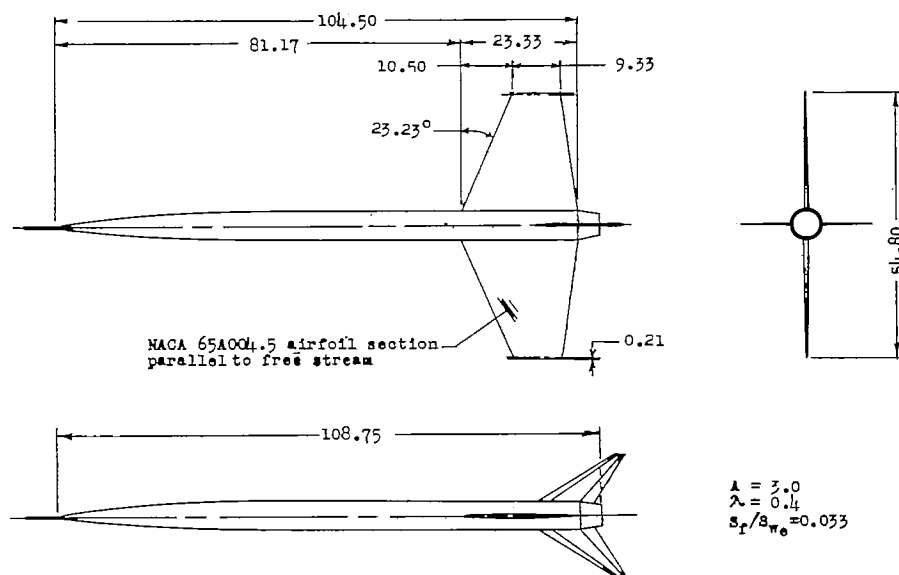
(c) 4.5-percent-thick, unswept, tapered wing (model 4).
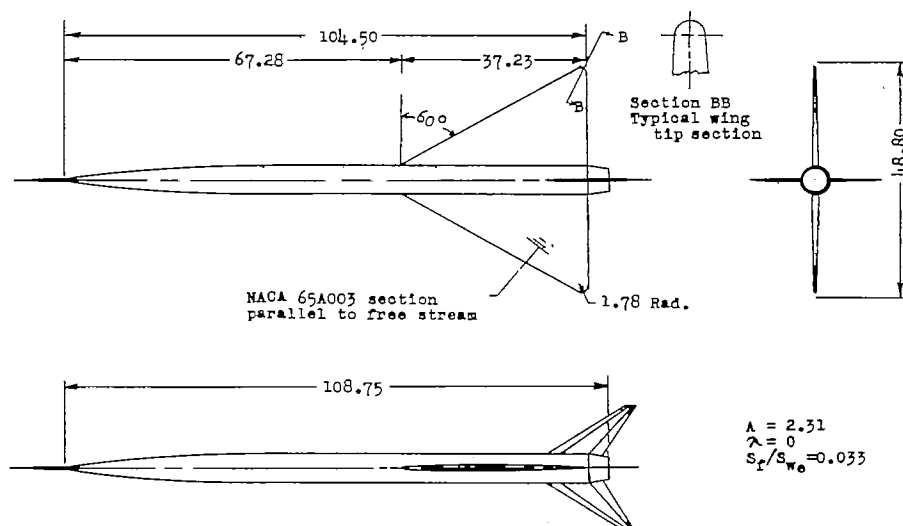
(d) 3-percent-thick delta wing (model 5).

Figure 1.- Continued.

104.50

67.28

18.61 ── 18.61

40.87°

NACA 65A003 airfoil section
parallel to free stream

1.94 Rad.

48.80

108.75
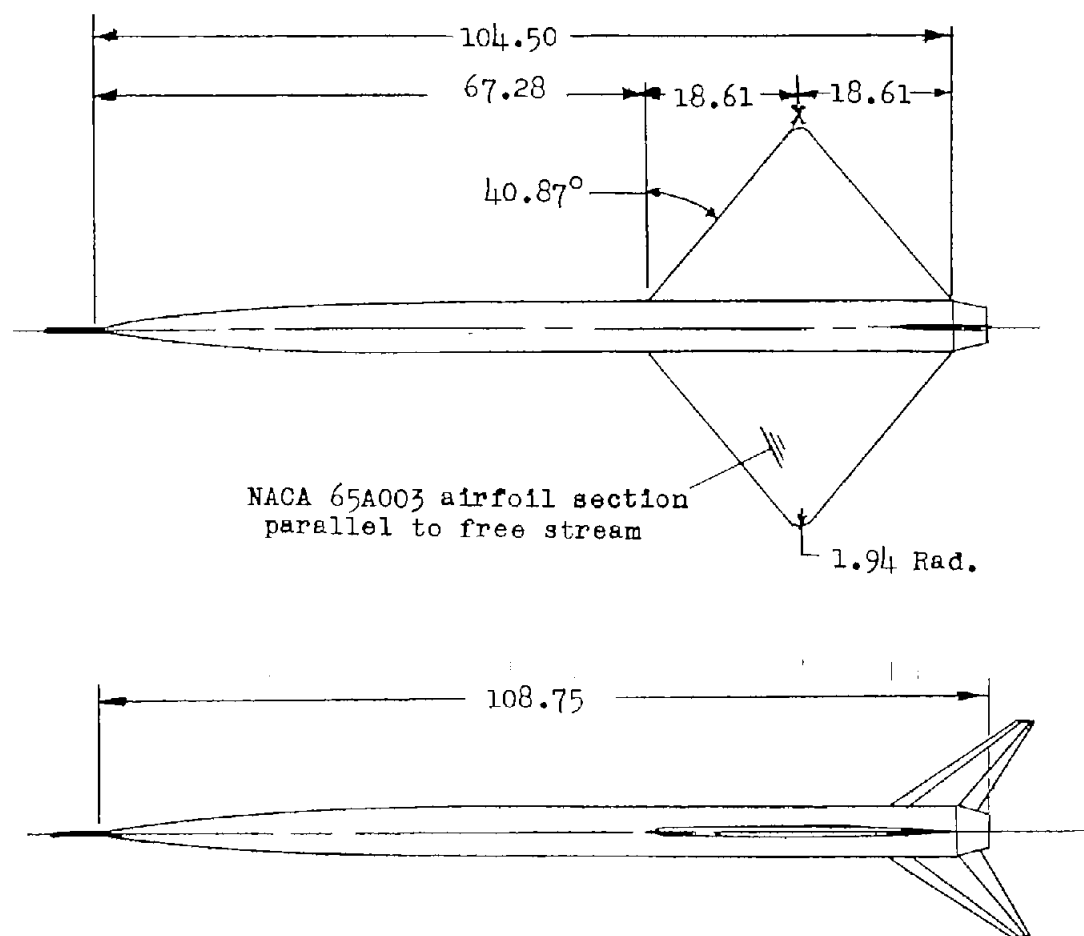
$A = 2.31$
$\Upsilon = 0$
$S_f/S_{w_e} = 0.033$

(e) 3-percent-thick diamond wing (model 6).

Figure 1.- Concluded.
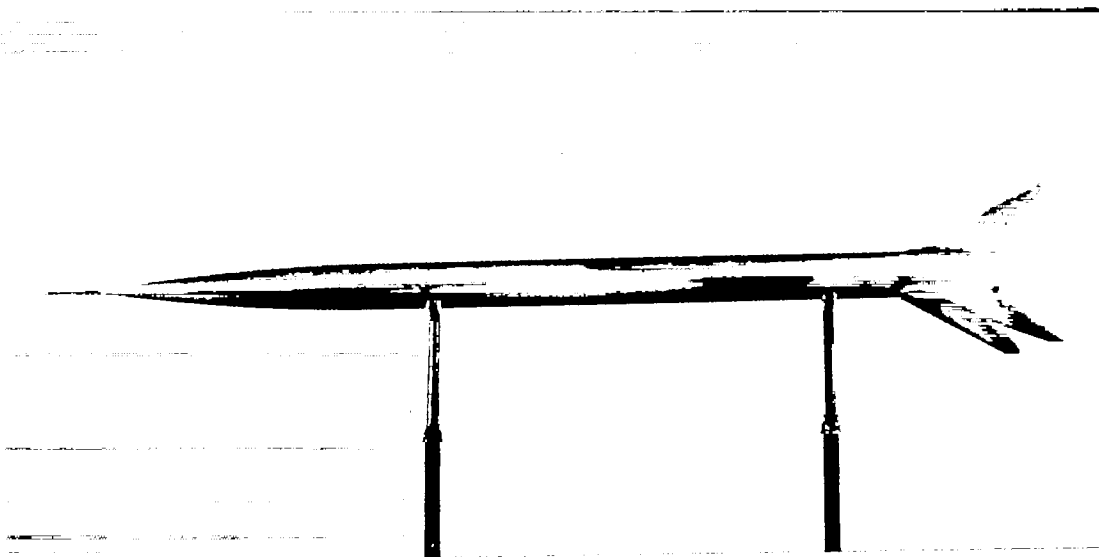
(a) Basic wingless body.   L-78909.1
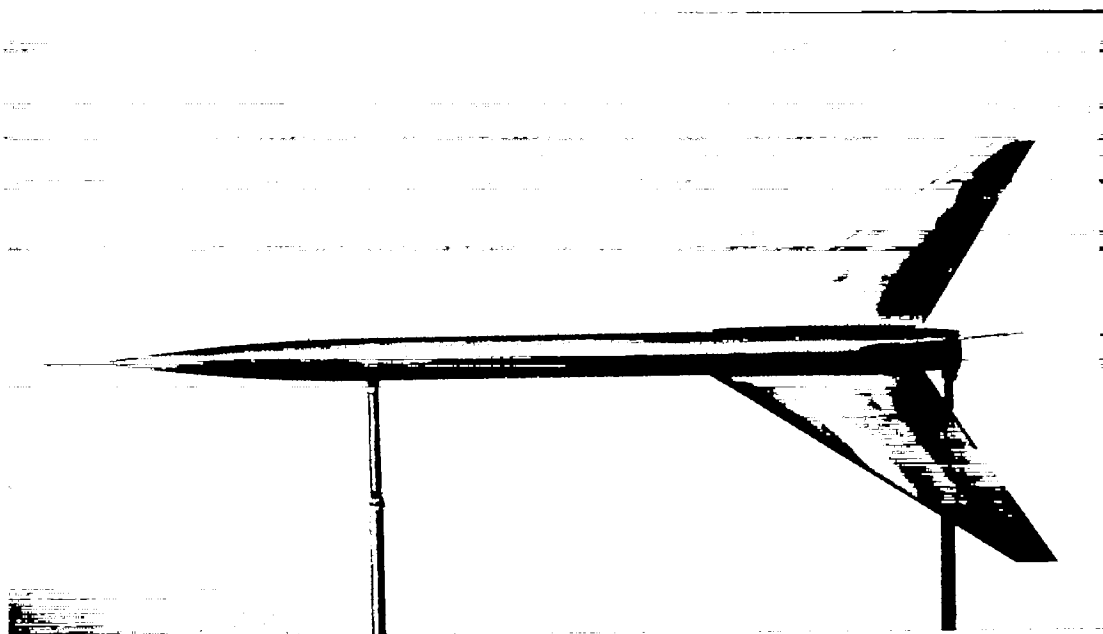
(b) Model 3.   L-84001.1

Figure 2.- Photographs of basic body and typical winged model.
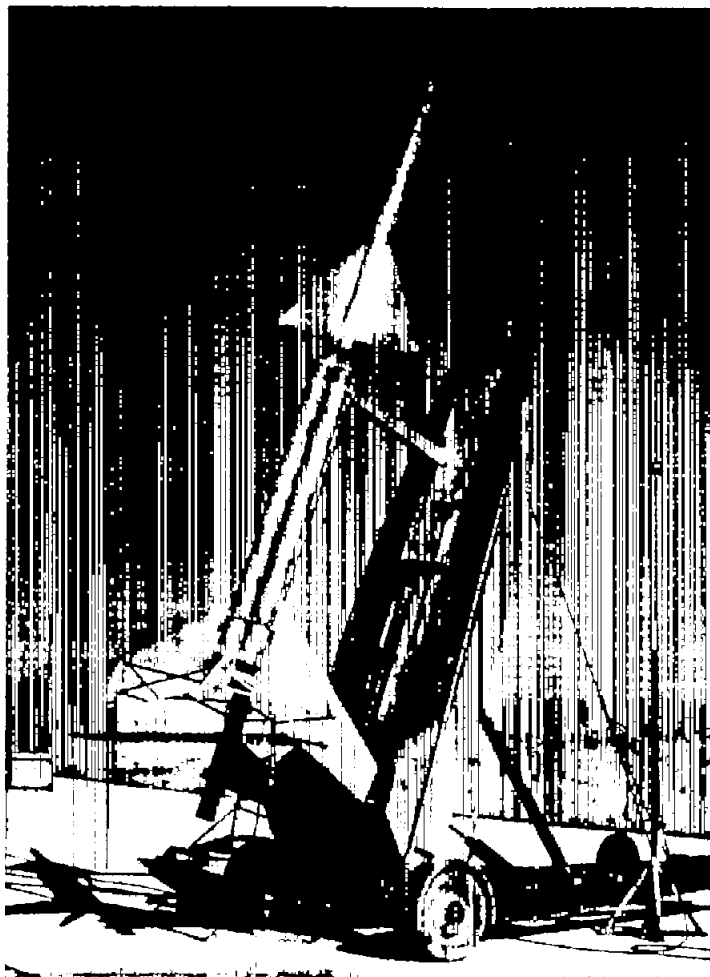
L-83986.1

(a) Model 5 with quadruple Deacon booster.

L-88028.1

(b) Model 6 with Nike booster.

Figure 3.- Typical model mounted for launching.

Base pressure manifold
$\frac{3}{16}$ I.D. tube

.064

.30

.3125   .30

.6125

4.40

5.00

Sta. 108.75

Base pressure orifice
4 equally spaced, 90° apart

.30
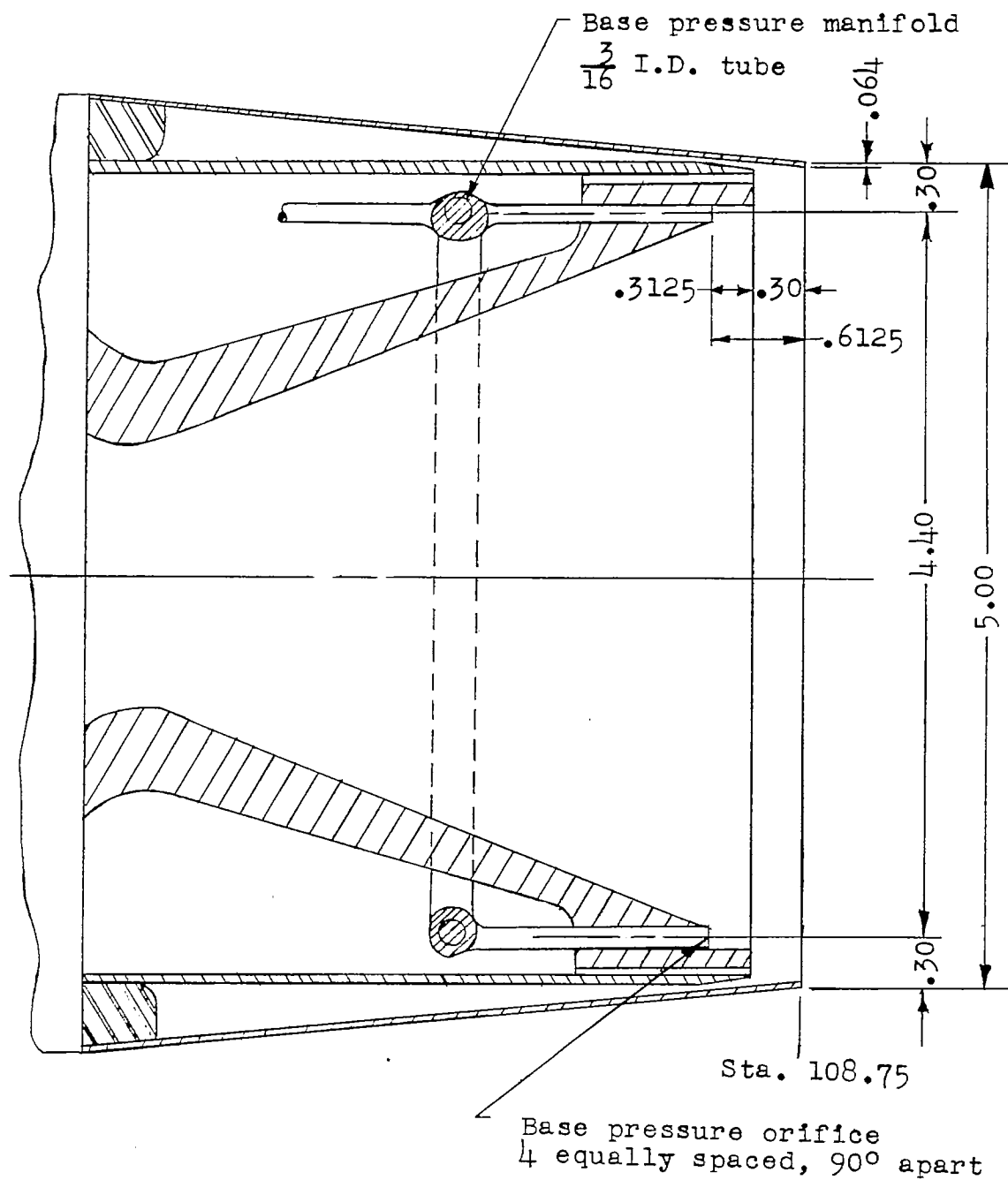
Figure 4.- Detail of base pressure orifice. All dimensions are in inches.
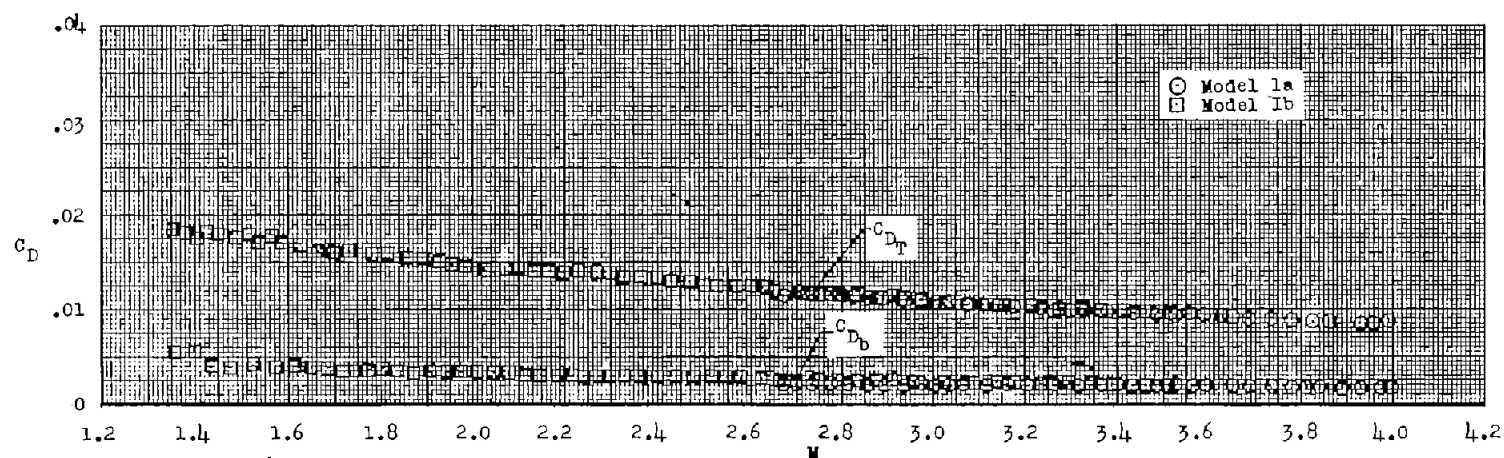
Figure 5.- Typical drag-data plot for one test configuration (models 1a and 1b). Drag coefficients
are based on exposed wing area, 5.556 square feet.
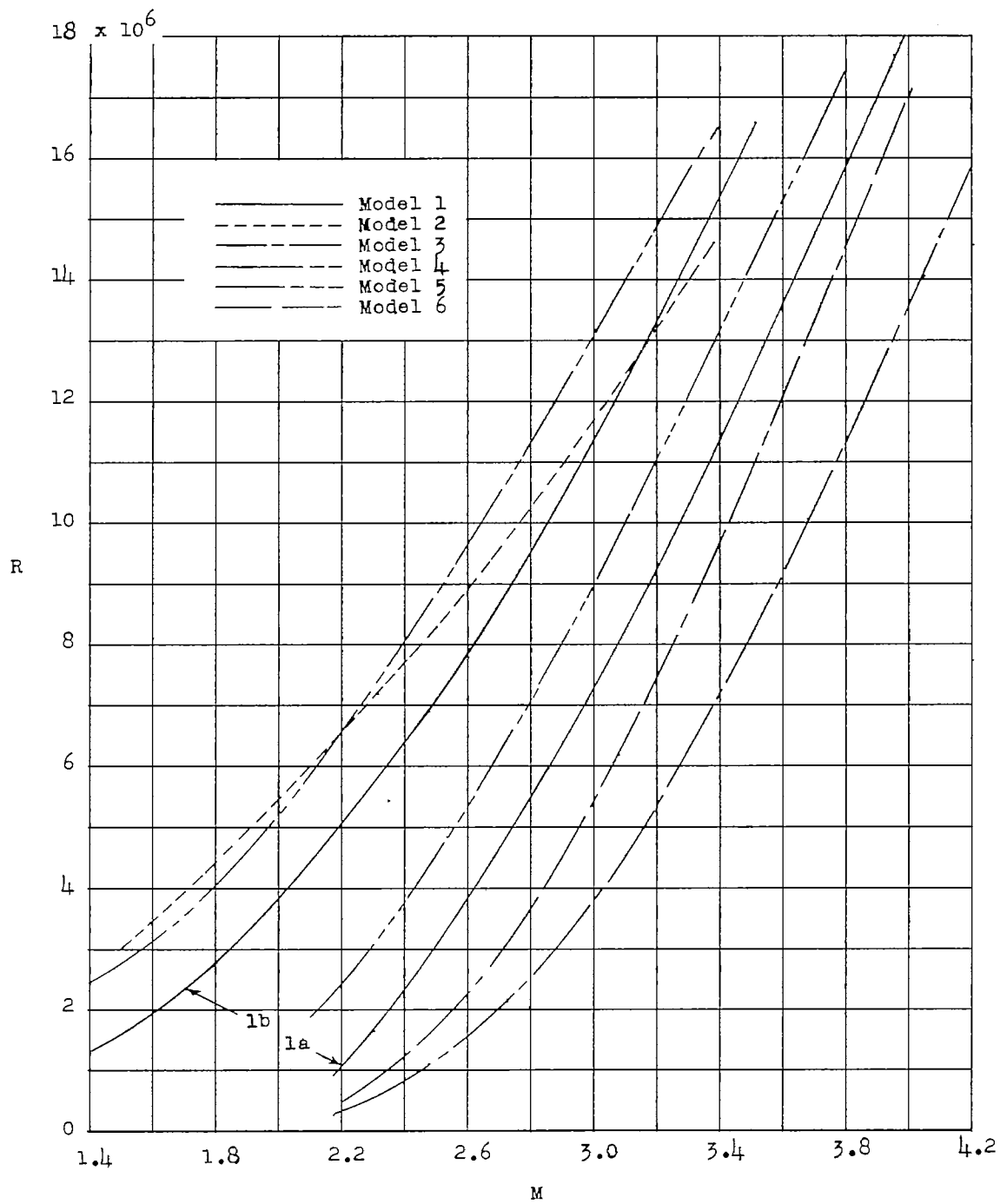
Figure 6.- Variation of Reynolds number based on a length of 1 foot with
Mach number for the various test models.
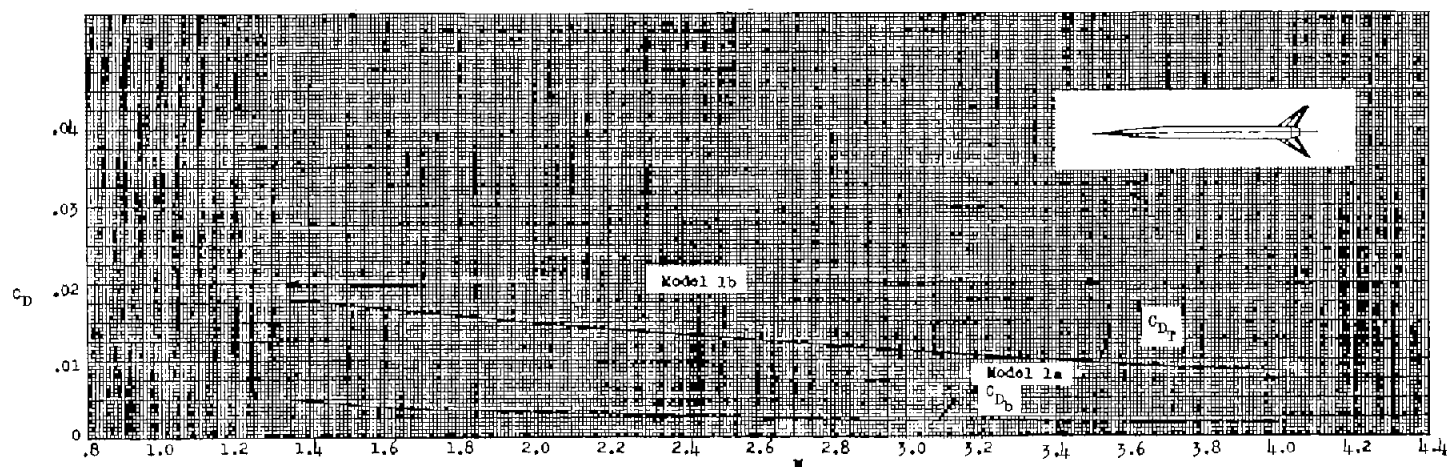
(a) Models 1a and 1b, basic body.
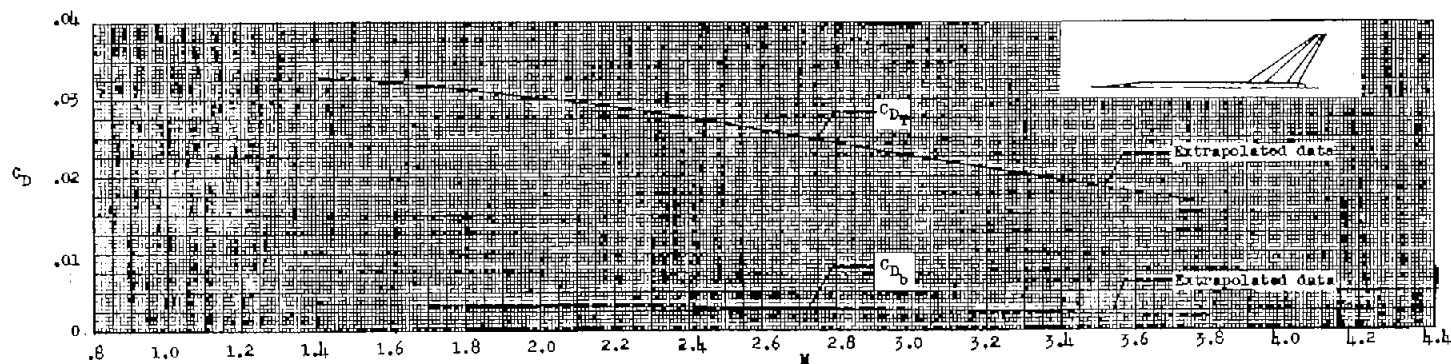
(b) Model 2; swept, tapered slab wing.

Figure 7.- Variation of total and base drag coefficients with Mach number for the test models. Drag coefficients are based on exposed wing area of 5.556 square feet.
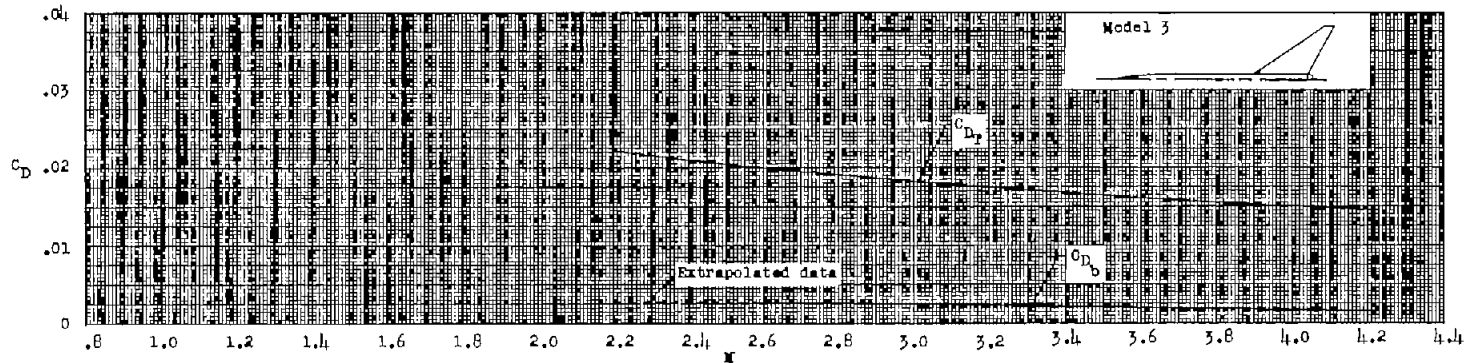
(c) Model 3; swept, tapered wing with NACA 65A004 airfoil section.
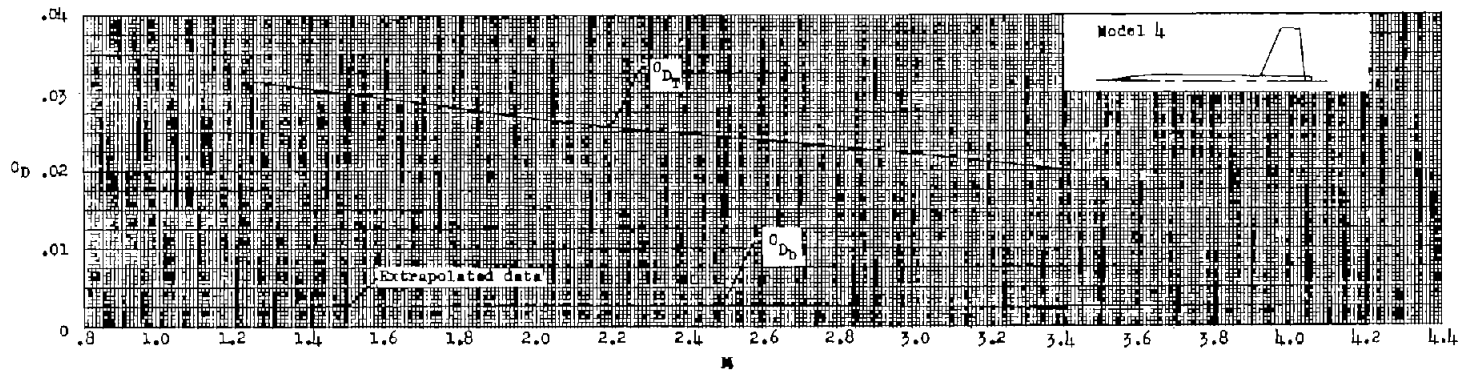
(d) Model 4; unswept, tapered wing with NACA 65A004.5 airfoil section.

Figure 7.- Continued.
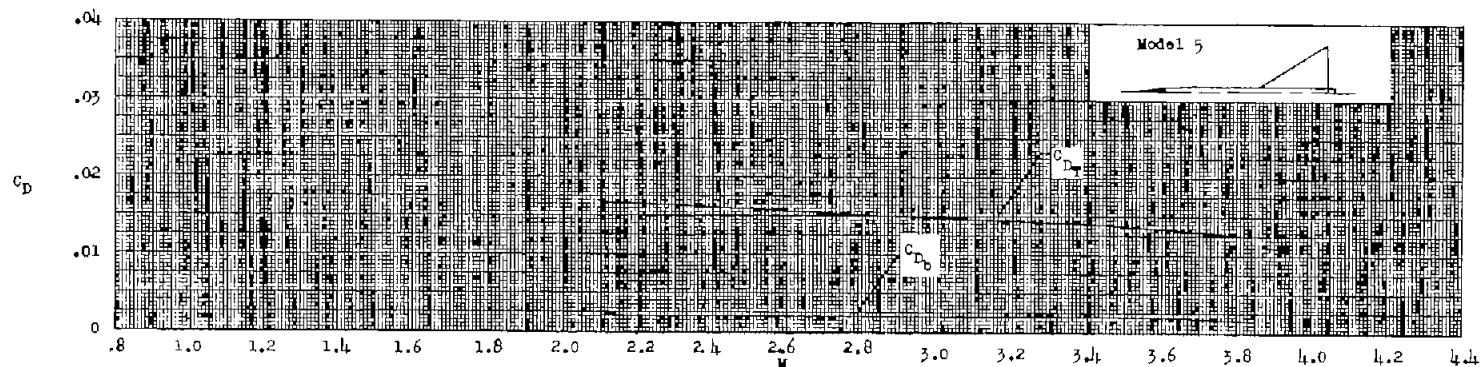
(e) Model 5; delta wing with NACA 65A003 airfoil section.
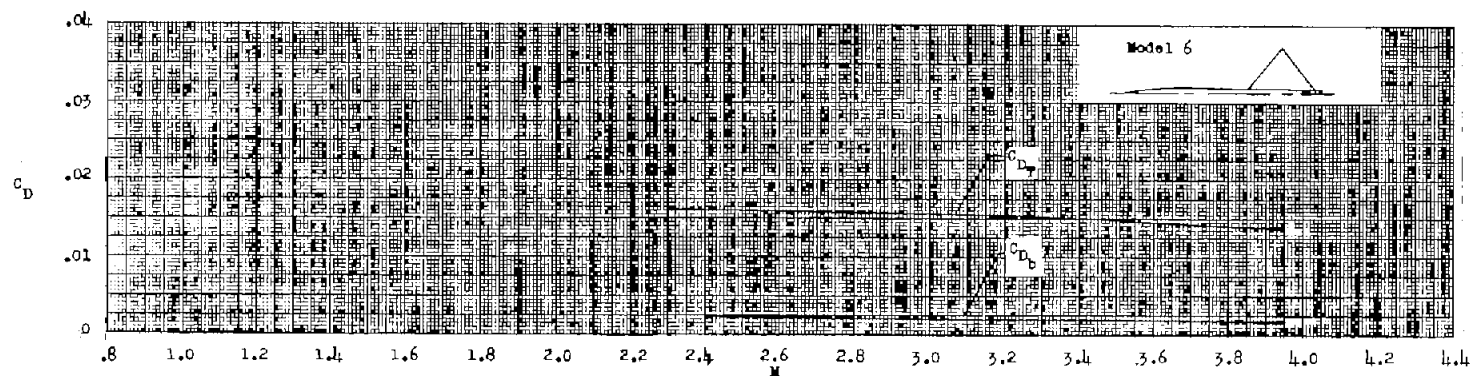
(f) Model 6; diamond wing with NACA 65A003 airfoil section.

Figure 7.- Concluded.
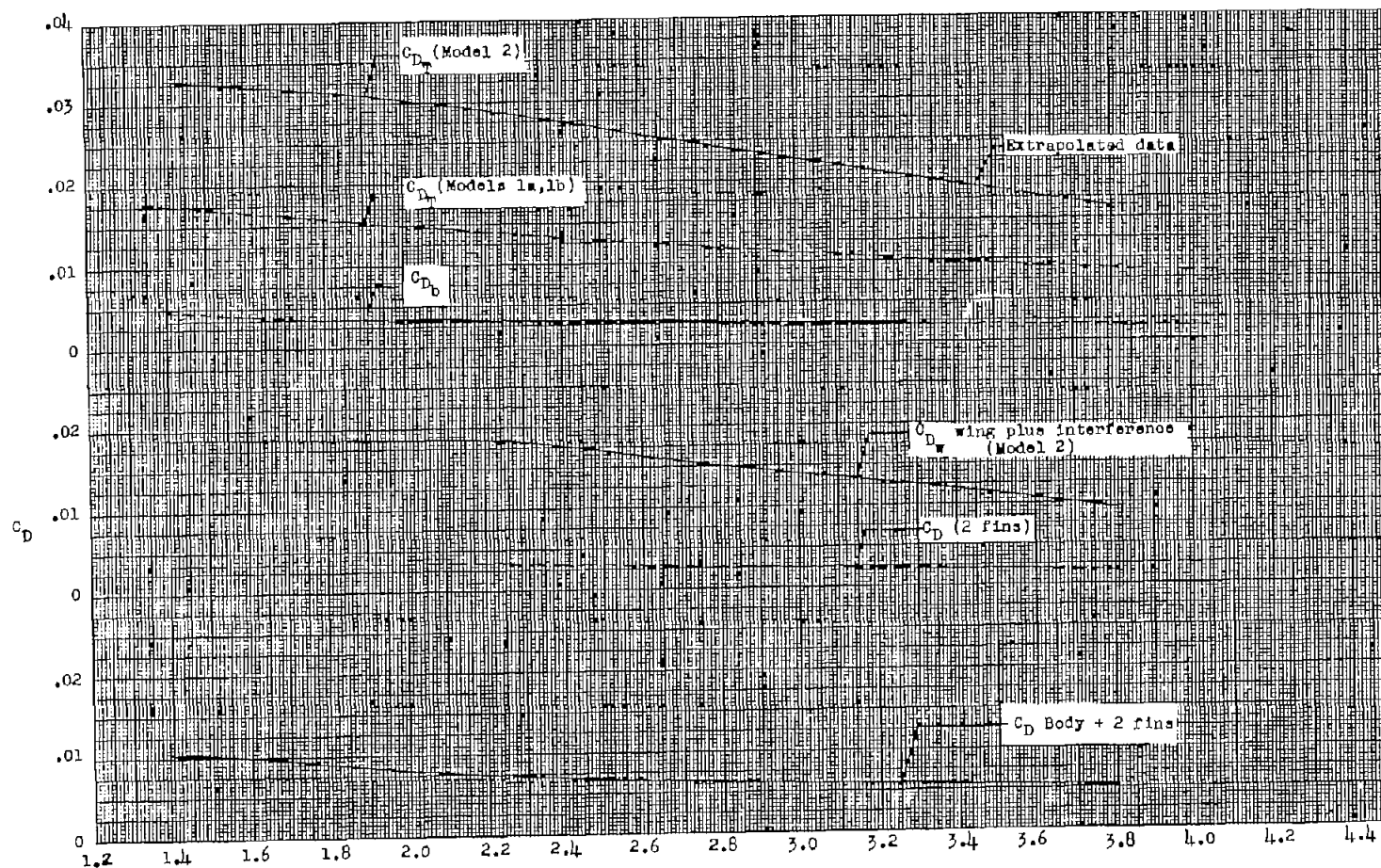
Figure 8.- Determination of experimental fin and body drag coefficients.
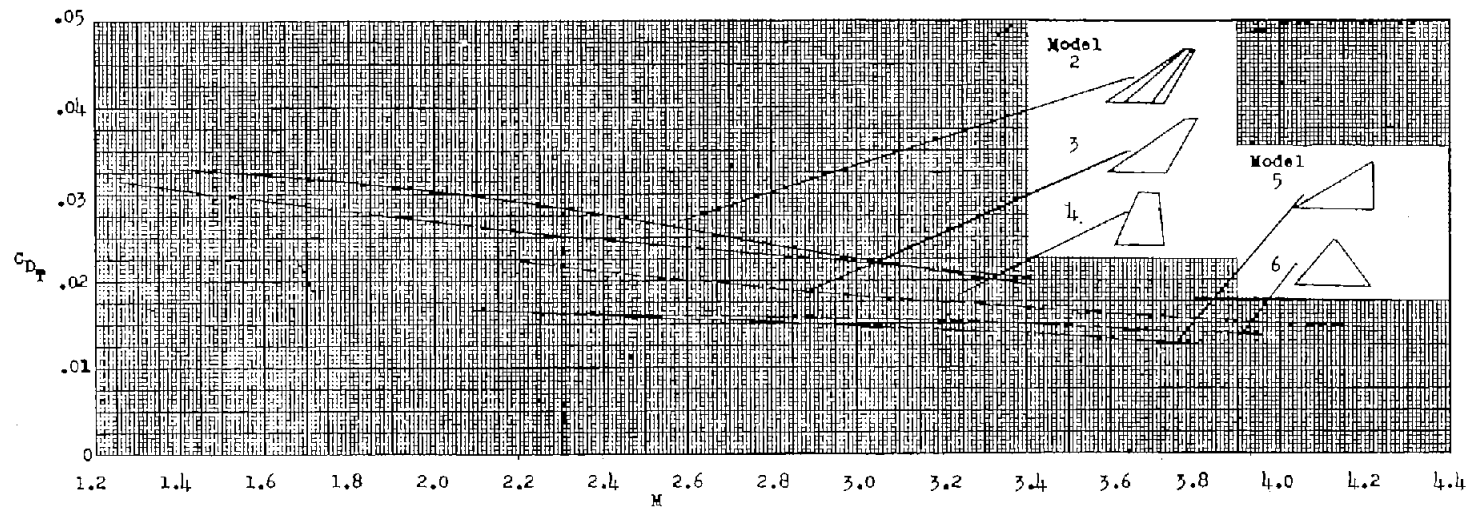
(a) Total drag coefficient.
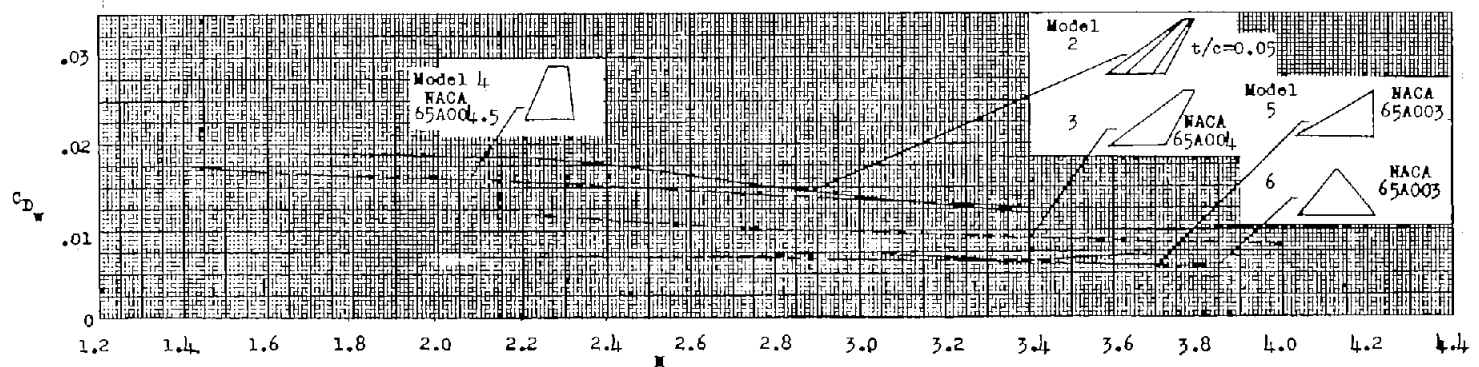
(b) Wing-plus-interference drag coefficient.

Figure 9.- Comparison of drag coefficients for the winged test models.
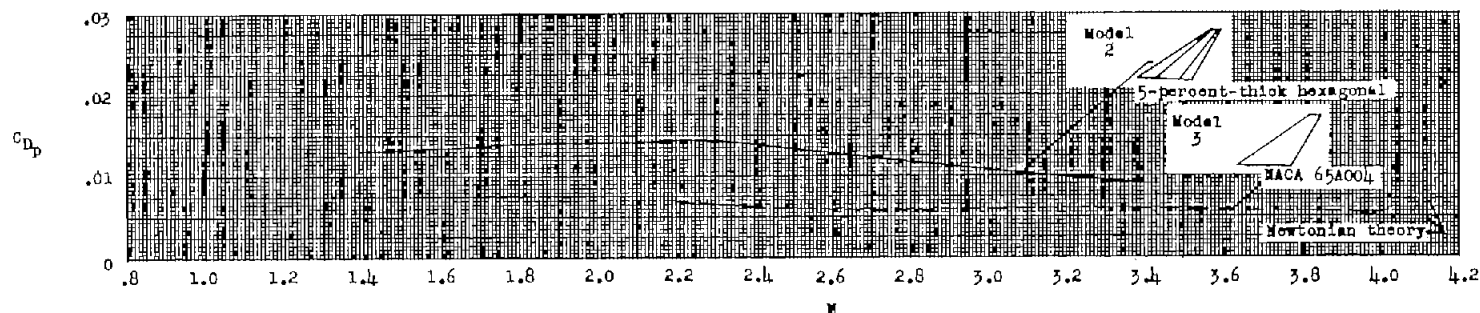
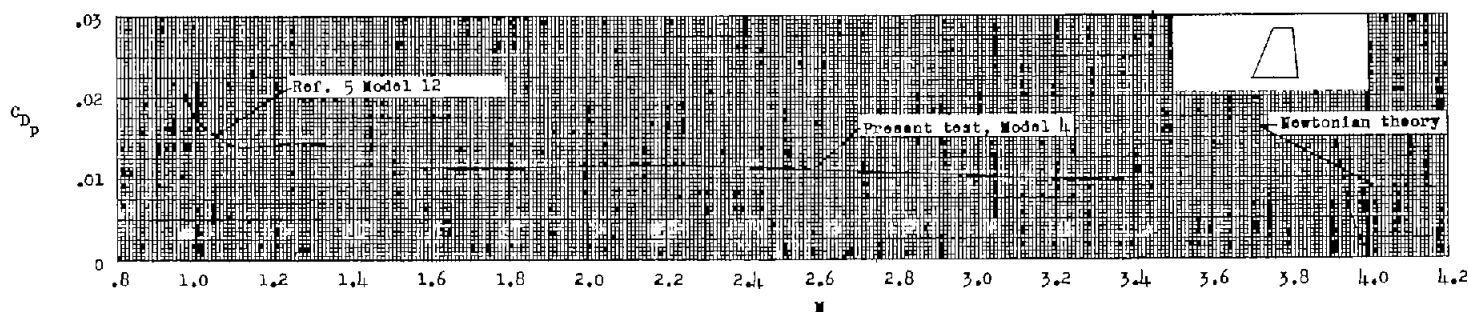Figure 10.- Comparison of wing-plus-interference drag minus calculated skin-friction drag for two swept, tapered wings of different airfoil section.

Figure 11.- Variation of wing-plus-interference drag minus calculated skin-friction drag for an unswept, tapered wing with an NACA 65A004.5 airfoil section.
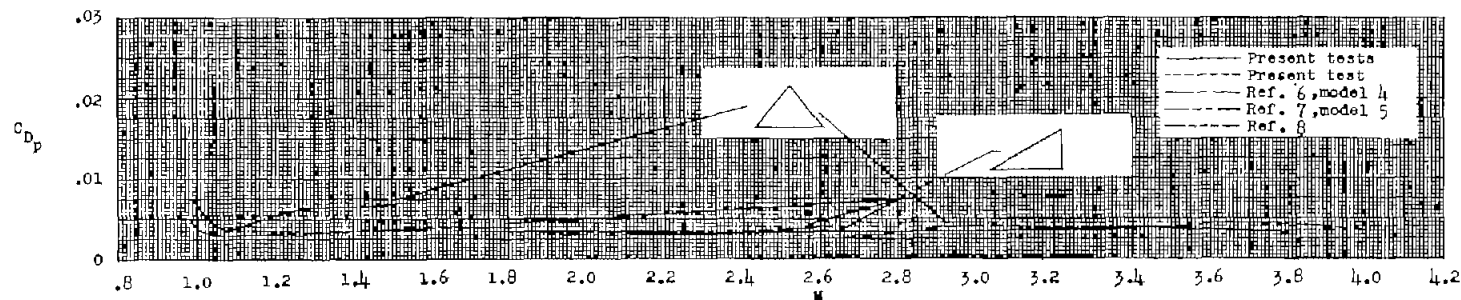
Figure 12.- Comparison of wing-plus-interference drag minus calculated skin-friction drag for a delta and diamond wing with 65A003 airfoil sections.
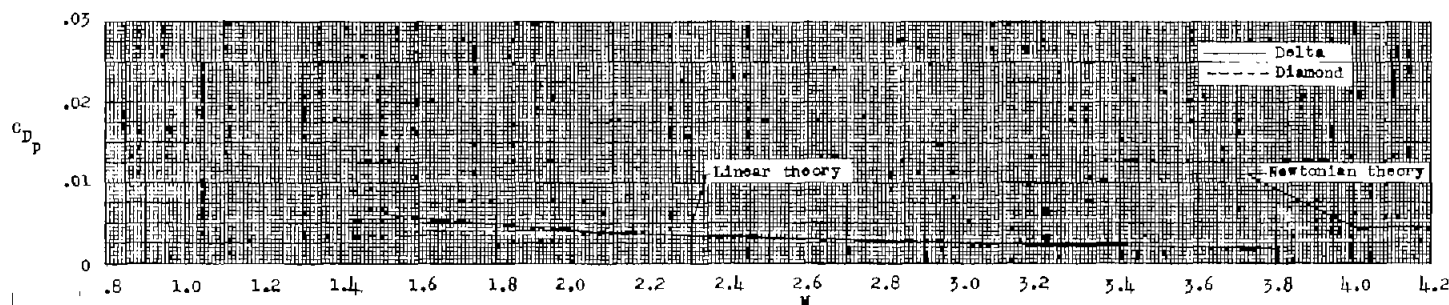

Figure 13.- Variation of theoretical wing pressure drag coefficient with Mach number for a delta and diamond wing with 65A003 airfoil sections.
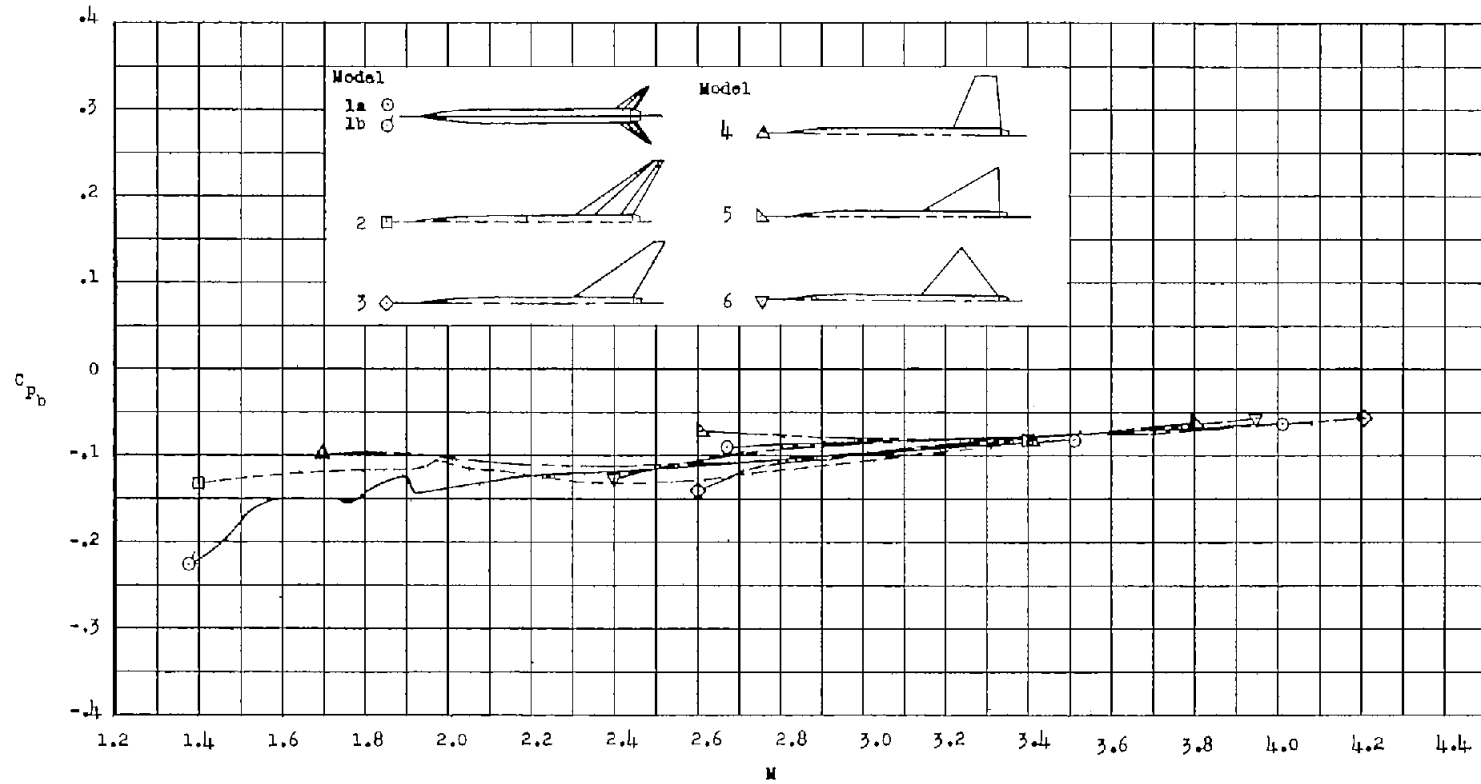
Figure 14.- Comparison of base-pressure coefficients for wingless and winged test models.